論文 / 著書情報
Article / Book Information

Title	Design of a 1:1 scale penguin-like robot with effective flexible wings
Authors	Yayi Shen, Zheming Ding, Bai Chen, Hiroto Tanaka
Citation	2023 IEEE 19th International Conference on Automation Science and Engineering (CASE), , ,
Pub. date	2023, 8
Copyright	(c) 2023 IEEE. Personal use of this material is permitted. Permission from IEEE must be obtained for all other uses, in any current or future media, including reprinting/republishing this material for advertising or promotional purposes, creating new collective works, for resale or redistribution to servers or lists, or reuse of any copyrighted component of this work in other works.
DOI	http://dx.doi.org/10.1109/CASE56687.2023.10260457
Note	This file is author (final) version.

Design of a 1:1 scale penguin-like robot with effective flexible wings

Yayi Shen, Zheming Ding, Bai Chen and Hiroto Tanaka

***Abstract*— Penguins are excellent swimmers benefiting from their streamlined body and agile wings. In order to realize such swimming abilities, a penguin-like robot at 1:1 scale was designed, mainly consisting of a streamlined body shell referring to the structure and size of real penguins, a pair of active wings, and a wing driving mechanism that can achieve flapping, feathering and pitch of the wings with a total of five degrees of freedom. The kinematic characteristics of the wings conforms to the anatomical conclusion. In addition, the bending deformation was measured over a dead wing specimen, and the flexural stiffness was calculated. Based on the results, a two-joint flexible wing was fabricated, which can undergo passive deformation during flapping. The performance of the fabricated wing is verified by water tunnel test. The results show that the flexible wing can achieve larger thrust forces and sideway forces, which indicate potential agile motion of the penguin-mimetic robot.**

***Index Terms*— Biomimetic aquatic robot, wing deformation, mechanism design, penguin robot.**

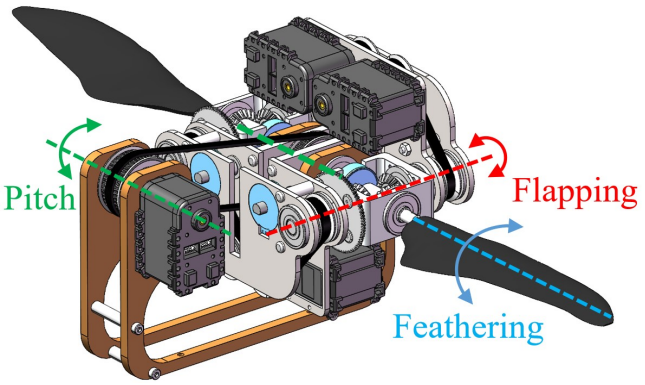

Fig. 1. A double-wing driving mechanism for the penguin-mimetic robot.

I. INTRODUCTION

Penguins have completely adapted to underwater life and have excellent swimming abilities. The swimming mode of penguins is the hydrofoil propulsion, which is based on a pair of flapping wings that can actively control the angle of attack (AoA). Compared with the oscillating fin propulsion which is an intermittent drag-based propulsion mode [1]–[3], the lift-based hydrofoil propulsion generates thrusts in the entire wing beat and has higher propulsion efficiency [4], [5].

Research on penguins' physiological structure reveals biological preconditions for their propulsion mode [6]–[9]. Raikow et al. studied the motion range of penguin elbow and wrist joints, Bannasch studied the structure and motion range of the penguin shoulder joint with cadavers. It has been reported that penguins have a ball-and-socket shoulder joint that allows penguin wings to perform flapping and feathering motion [9]. Moreover, the wings are almost fully extended during swimming [6]. AoA has a great effect on thrust generation. Penguin wings can achieve both propelling, maneuvering, and even effective force control through active AoA control. A recent anatomical study reported that there is no skeleton extending to the trailing edge of a penguin flipper, which leads to high flexibility of this region [8]. Besides, the variable AoA in the chord direction gives a possibility that penguins can use this feature to suppress excessive AoA at the wing tip to generate more thrust, which indicates that a flexible wing may have better propulsion performance compared with a rigid one.

The kinematics of penguin wings have also been revealed from various aspects [10]–[12]. A previous study reported that both upstroke and downstroke of the flapping wings can generate effective thrusts [12]. It is believed that penguins produce a vertical downward force to counteract buoyancy during swimming [10], which is quite different from birds flying in the air. The role of penguin upstroke in thrust generation is emphasized. The 2-D side-view motion analysis of forward swimming penguins in a water tank showed that lift-based thrust can be generated by a combination of feathering and flapping [13]–[15]. On this basis, we performed 3-D motion measurements on a real penguin and revealed quantitative 3-D wing kinematics [16]. As a result, it was found that the basic wing kinematics relative to the body mainly consists of obliquely straight flapping with spanwise feathering, while sweeping motion was found to have little impact on thrust [17]. The flapping motion and the feathering motion follow sinusoidal curves and the phase of feathering motion lags behind that of flapping motion by $\pi/2$ [18]. To the best of author's knowledge, it is the first time that these data have been obtained through quantitative measurements of real penguins, which provides an important bionic reference for the following research of hydrofoil robots.

In the robotics field, underwater bionic robots have been widely concerned due to their high energy efficiency, motion stability, maneuverability and noiseless motion [19]–[21]. Previously, bionic robots imitating fish and dolphins have been investigated in a lot of research. Some robots mainly

This work was partially supported by the Natural Science Foundation of Jiangsu Province (Grant No.BK20220892) and the JSPS KAKENHI Grant-in-Aid for Scientific Research on Innovative Areas (JP18H05468). (*Corresponding author: Hiroto Tanaka.*)

Yayi Shen, Zheming Ding and Bai Chen are with the College of Mechanical & Electrical Engineering, Nanjing University of Aeronautics and Astronautics, Nanjing, People's Republic of China(e-mail:yayi.shen@gmail.com).

Hiroto Tanaka is with the Department of Mechanical Engineering, Tokyo Institute of Technology, Tokyo, Japan(e-mail:tanaka.h.cb@m.titech.ac.jp).

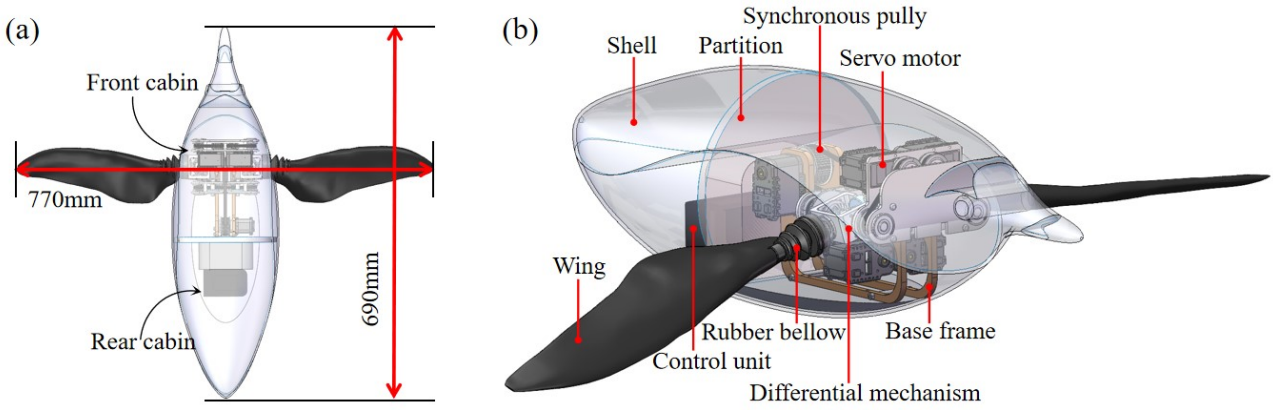

Fig. 2. Illustration of the 1:1 scale penguin-like robot: (a) Size of the penguin robot; (b) Internal structure of the penguin robot.

rely on their caudal fins to generate thrust [22]–[24], while the others have hydrofoils similar to penguin. But there is no more discussions on active AoA or flexible wings [25]–[27]. FESTO developed a bionic penguin called "AquaPenguin" ten years ago, which can achieve active flapping motion and passive feathering deformation with a pre-fixed amplitude [28]. Liu et al. developed a pair of flexible foreflippers, which can realize a movement similar to the front fin movement of sea lions [4].

In our previous research, based on the results of 3-D motion measurements, we decomposed the wing motion of the penguin into three DoFs: flapping, feathering and pitch. A 3-DoF robotic penguin wing that is capable of actively controlling flapping and feathering angles and flapping direction was developed to evaluate the thrust performance through water tunnel experiments. The subsequent study on penguins' turning swimming has also proved the importance of the 3-DoF control the wing motions [29]. The driving mechanism of the robotic penguin wing is composed of two main parts. The differential gear part consists of a differential and auxiliary transmission structures, which is powered by two servo motors to realize flapping and feathering motion. The whole differential gear part is connected to the fixed frame, which is driven by another servo motor independently to realize pitch motion. The results showed that large instantaneous thrust can be generated through the combination of smaller flapping amplitude and smaller feathering amplitude, feathering motion can prevent stall and pitch motion can effectively alter the thrust direction. Detailed description of the mechanism and introduction of the experiments can be found in another published paper [18].

However, the original one-wing driving mechanism was developed for evaluation of the wing motion and the thrust characteristics. The mechanism was not compact enough for a 1:1 scale penguin-like robot. Hence, we optimized the structure and developed a compact double-wing driving mechanism in this paper (as shown in Fig. 1), which can realize independent control of the flapping and feathering of each wing and simultaneous control of the pitch motion of both wings. Note that the wings in Fig. 1 are at 0.6-scale considering the page space. A penguin-like body shell was used for isolating the control unit and the driving mechanism from the water outside. Moreover, we developed a two-joint flexible wing based on the flexural stiffness of real penguin wing. The thrust performance will be compared with the rigid wing.

The remainder of this paper is organized as follows. In Section II, the design of the penguin robot including the optimized driving mechanism is introduced. The measurement on a real penguin and the implementation of an artificial flexible wing are explained in Section III. Discussion and conclusion are summarized in Section IV.

II. DESIGN OF THE PENGUIN ROBOT

We intend to make an underwater vehicle that can achieve agile swimming as a penguin. Excessive body size will limit the agility of the robot. The robot that we envision has a size similar with a real penguin. A pair of active wings are also necessary for generating large torques and complex swimming motions, which requires us to redesign the structure of the wing mechanism based on the expected size. We first designed the body shell of the penguin robot. The shape, the size and the material were determined. Then, the wing mechanism was designed so that it can be completely wrapped by the shell and the expected wing motion can be achieved.

A. Robot Body at 1:1 Scale

We first considered the design of the body shell since it determines the size and layout of other internal structures. We made a shell model of the penguin body with reference to the size of the real penguin. As shown in Fig. 2(a) of the 3-D model of the robot, the length of the body shell is 690 mm and the whole wingspan is 770 mm The length of the real penguin in the previous 3-D motion measurements is near 0.7 m [18]. The body shell is designed to be streamlined for better hydrodynamic performance. Notably, motions of penguin feet, the tail and the spine can have influences on the swimming postures of penguins. Given that these parts have little effect on the thrust performance in the process

of penguin swimming [14], they were not considered during the robot design in this paper to reduce the complexity and highlight the impact of penguin wings. The body shell is made from tough PLA, which means it is rigid and the head or spine cannot be actively deformed. In order to reduce the weight of the penguin robot and ensure the strength of the shell, the thickness of the shell is determined to be 3 mm.

Beside the body shell, there are two rubber bellows that closely connect the body shell with the wings at the root part, which prevents the water form going inside the body shell meanwhile allows the movement of the wings. We fabricated a stable platform which bottom shape is consistent with the inner surface of the shell, which can closely fit with the shell bottom and have a flat upper surface. It is placed at the bottom of the robot as a support for other parts. The space of the body shell is divided into the front cabin and the rear cabin by a rigid partition: the driving mechanism including the motors are in the front cabin; the control unit and the power source are placed in the rear cabin. Large space is reserved at the rear of the robot, and other functions can be combined if necessary. The internal structure of the robot body is shown in Fig. 2(b).

B. Double-wing Driving Mechanism

The position of the bionic penguin wings relative to the body shell is determined according to the conformation of real penguins. As shown in Fig. 2(a), penguin wings locate at the front of the body, which is different from marine organisms that rely on median and paired fin (MPF) mode to promote, such as manta rays. Due to the limitation of the streamlined structure and the body size, the front part of the penguin robot is very narrow, which means limited space is reserved for the driving mechanism.

In the original 3-DoF robotic penguin wing, the feathering motion and the flapping motion are coupled through a differential gear system driven by two servo motors, while the pitch motion is controlled by another motor independently. Main thrusts are generated by the flapping motion and the feathering motion, while the pitch motion controls the direction of the thrust. This mechanism was designed based on the penguin bionics and the decoupling of pitch motion reduces the difficulty of control for flexible 3-D motion. As shown in Fig. 3(a), we retained the employment of the differential gear mechanism to generate the flapping motion and the feathering motion, as this part has been shown to be effective and reliable in previous experiments. However, some improvements are needed, including shortening the length of the transmission shaft and reducing the distance between the differential gears and the base frame. At the same time, the pitch mechanism was improved for better compactness.

As shown in Fig. 3(a), the optimized double-wing driving mechanism is designed to be approximately symmetrical about the base part. The differential gear mechanism for each wing is fixed on each side of the base frame. Four servo motors (two for one wing) are used to actuate the flapping and feathering motion of both wings. The layout of the motors has been carefully designed, which have high efficiency in space utilization and reduce the spanwise distance of the robot. The structure of the differential gear mechanism is basically unchanged, which means that the generation of the flapping motion and the feathering motion can follow the previous motion equations and control parameters. In this mechanism, the main function of the pitch motion is to control the thrust direction rather than coupling it with

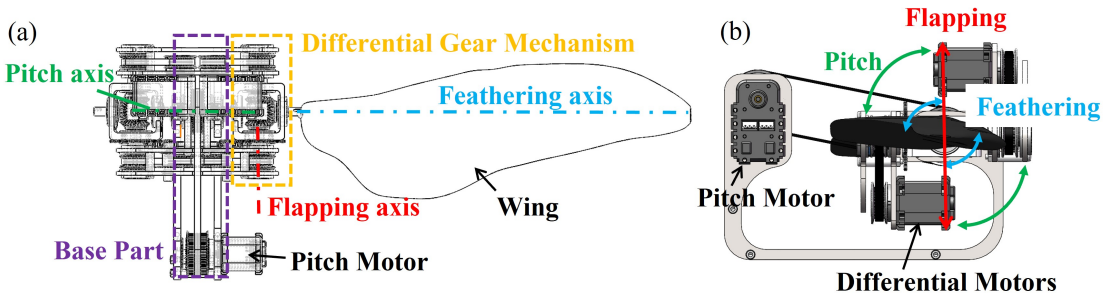

Fig. 3. (a) Schematic drawing of the driving mechanism (top view); (b) Side view of the driving mechanism.

TABLE I
COMPARISON OF THE WING'S MOTION RANGE

Description	Elevation	Depression	Pronation	Supination
Anatomical results [9]	45°	No restriction	53°	39°
3D motion measurement results [16]	36.2°	39.9°	25.7°	6.9°
Designed double-wing driving mechanism	50°	50°	90°	90°

the flapping motion. We unified the pitch motion of the wings on both sides for simplification. As seen in Fig. 3, the pitch motor is installed at the rear of the differential gear mechanism, and a notch in the middle of the base frame leaves space for the synchronous belt to realize pitch actuation. In brief, one pitch motor, two flapping motors and two feathering motors are utilized for actuating the whole robot. Besides, there are some changes in details, such as re-selection of the motor and potentiometers, modification of the gearbox, *et al*.

The 3-D model of the optimized driving mechanism is shown in Fig. 1, where the red line in the figure represents the axis of the flapping motion of the right wing, the blue line is the axis of the feathering motion of the right wing, and the green lines represent the axes of the pitch motion. For clear view, only the axes of the right wing were depicted. Both the rotational axis of the wings and the drive axis of the motor are marked with respect to the pitch motion. The driving mechanism can be completely covered by the pre-designed robot body, and the motion angles of the flapping, feathering and pitch can achieve sufficient ranges. The comparison among the motion range of the designed mechanism and the results obtained from anatomy [9] and the 3-D motion measurements [16] is listed in Table I. The elevation represents the wing flapping upwards, the depression represents wing flapping downwards, the pronation represents the wing leading edge rotating downwards, and the supination represents the wing leading edge rotating upwards. It is seen that the double-wing driving mechanism can realize sufficient motion ranges of the wing.

III. IMPLEMENTATION OF THE FLEXIBLE WING

Penguins are observed to bend and twist their wings during swimming. Our previous research have revealed that the wing bending can result in smaller angle of attack of the outer wing so as to larger thrust [16]. Hence, we measured the flexural stiffness of a penguin wing specimen. Based on the results, an artificial flexible wing was fabricated for more efficient robotic application.

A. Flexural Stiffness of a Penguin Wing Specimen

To obtain the flexural stiffness of the penguin wing, we measured the deformation of a right wing specimen (as shown in Fig. 4) in different load situations. The specimen came from a dead rockhopper penguin (*Eudyptes chrysocome*) and was stored in a refrigerator. Before the measurement, the specimen was unfrozen at room temperature. It should be noted that the dead organism can result in varied characteristics of the wing from living penguins. Besides, the measured wing specimen was limited to one penguin individual and the torsional deformation was not considered in this report.

As shown in Fig. 4(a), sixteen markers were attached along the leading edge and the trailing edge of the wing. The displacements of the markers were recorded while applying vertical forces at the wing tip. The wing coordinate is depicted in the figure and a schematic drawing of the

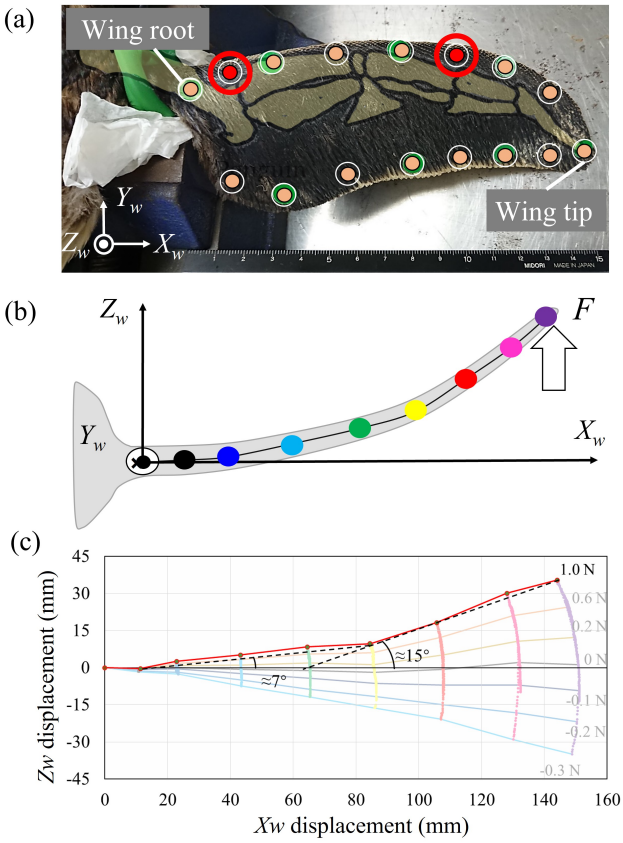

Fig. 4. Bending deformation measurement of the wing specimen: (a) the penguin wing with attached markers; (b) schematic drawing of the measuring process; (c) results of the wing deformation measurement.

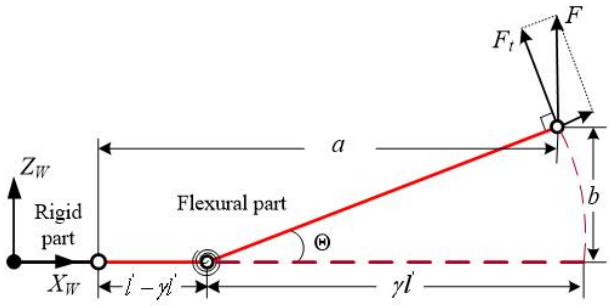

Fig. 5. Bending model of the wing in PRBM

measuring process is seen in Fig. 4(b). Fig. 4(c) shows each marker position while applying different loads F to the wing tip. It can be seen that larger force was needed to lift the wing upward than to push downward, which means the flexural stiffness of the wing was not symmetric about the wing surface. Moreover, obvious displacement can be found at the second and sixth marker form the wing root when lifting upward. In contrast with the bone structure of the wing shown in Fig. 4(a), both markers correspond to the wing joint.

The flexural stiffness of the wing was calculated using the pseudo-rigid-body method (PRBM), where we assume

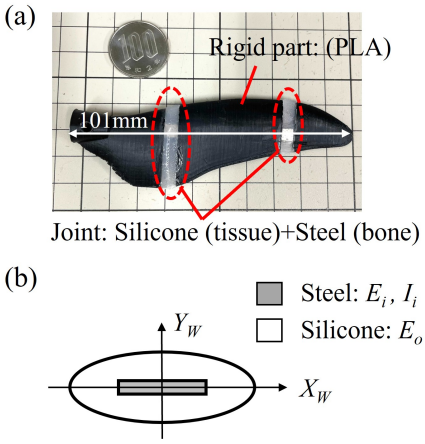

Fig. 6. (a) Fabricated flexible wing with two elastic joints; (b) cross section showing the structure of the elastic joint.

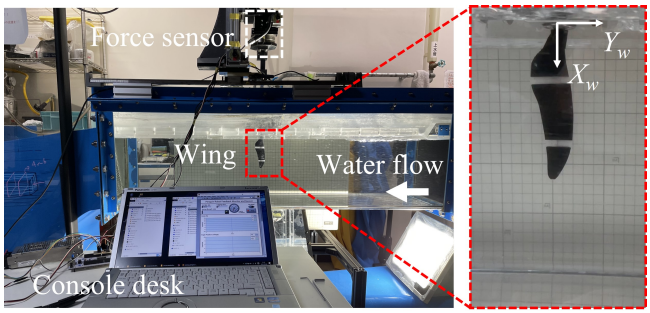

Fig. 7. Experimental setup for measuring the hydrodynamic forces.

the wing with elliptical cross section and average flexural stiffness. As shown in Fig. 5, the wing was composed of the rigid part and the flexural part. The flexural part was modeled as two rigid links connected by a torsional spring with the constant of K_Θ. When applying the load F to the pseudo-rigid-body, it was obtained:

$$F_t = \frac{EIK_\Theta\Theta}{l'^2} = F\cos\Theta \tag{1}$$

where F_t indicates the perpendicular component of load F, EI is the average flexural stiffness, Θ is the pseudo-rigid-body angle, and l' is the length of the flexural wing part. The pseudo-rigid-body angle Θ can be calculated by:

$$\Theta = \tan^{-1}\frac{b}{a - l'(1-\gamma)} \tag{2}$$

where the displacements a and b can be determined through the position of the wing tip.

B. Fabrication of an Artificial Flexible Wing

Since two evident joints were found in previous section, the artificial flexible wing was designed as three rigid segments connected by two elastic joints. As shown in Fig. 6(a), the rigid parts were printed with a 3D printer using PLA material. The joint was composed of the inner material steel which worked as the bone, and the outer material silicone which worked as the tissue. Considering the water tunnel tests of the thrust performance, 0.4-scale of the wing was fabricated in this report. Therefore, the tested flexible wing measures 101mm, which was the same as the rigid wing in our previous research. The cross section of the joint was shown in Fig. 6(b). It was simplified as an ellipsoid silicone enclosing a rectangle steel. As a result, the flexural stiffness can be calculated by:

$$k = E_oI_o + E_iI_i \tag{3}$$

where E_o and E_i indicate the Young's modules of the outer material (silicon) and the inner material (steel), respectively, I_o and I_i are the area moments of inertia of the outer material and the inner material. In our tests, the outer material was the Dragon skin 10 fast silicone with the E_o of 181 kPa, and the stainless steel with the E_i of 180 GPa was used as the inner material. A rectangular steel measuring 0.4 mm thickness and 5 mm width was employed as the inner bone.

C. Experimental Verification

To verify the thrust performance of the fabricated flexible wing, a force measurement setup (shown in Fig. 7) was built above the water tunnel measuring 1×0.2×0.3 m^3.During all tests, the flow speed of the water tunnel was set to be constantly 1 m/s. To compare the thrust performance between the rigid and the flexible wings, both wing models were actuated to follow the same motion in the water flow. The flapping amplitude was set as 40° and the frequency was 2.2Hz. We varied the feathering angle at a range from 0 to 40° to change the angle of attack, which allowed us to observe different thrust situations. These conditions resulted in a Strouhal number of 0.277 and an average Reynolds number of 28000.

The results are shown in Fig. 8. Effective force was used as the metric for comparing between the rigid and the flexible wings, which can be calculated by $N_x = 1/T\int_0^T F_{x,y}(t)dt$, where T denotes the duration of the wing motion and $F_{x,y}(t)$ indicates the forces measured along the X_w-axis (sideway force) and the Y_w-axis (thrust force). It can be seen that the thrust forces of both wings reached to a maximum value when the feathering amplitude became larger, then started to decrease after the peaks. Moreover, the maximum effective thrust force of the flexible wing is larger than the rigid one. The thrust force also increases faster than the rigid wing before the maximum values. As for the sideway force, the flexible wing generated larger absolute forces for most of the feathering amplitudes. The force directions of both wing models varied when increasing the feathering amplitude.

IV. CONCLUSIONS

Penguins are capable of fast swim and high mobility, which mainly relies on their streamlined body and agile wings. In this paper, a 1:1 scale penguin-like body referring to the real penguin is designed and the driving mechanism of a pair of wings is optimized. The robot can realize independent control over the flapping and the feathering motion of each wing, and the pitch of both wings at the same time. The mechanism allows the wings to move within the

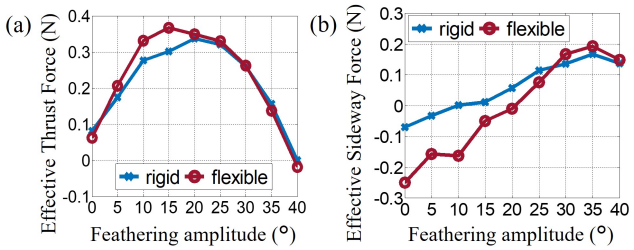

Fig. 8. Thrust performance comparison between the rigid wing and the fabricated flexible wing: (a) effective thrust force in the Y_w-axis; (b) sideway force in the X_w-axis.

range of anatomical conclusions and the position of penguin wings is adjusted to approximate the real situation.

On the other hand, the bending deformation of a penguin wing specimen was measured and the flexural stiffness was obtained. Based on the results, a two-joint flexible wing was fabricated to compare with the rigid wing. We analyzed the thrust force and the sideway force generated by both wings. Experimental results showed that the wing bending does have an impact on thrust generation. When the feathering amplitude increases, the flexible wing have higher thrust growth and peak thrust compared with the rigid wing. The results are also consistent with the previous findings of aquarium penguins that the wing bending can lead to better thrust performance. Moreover, the flexible wing is able to generate larger sideway force, which makes the robot more possible to realize complex maneuvers like fast turning.

In the future work, both bending and torsional deformation of the wing will be considered. The designed 1:1 scale penguin-mimetic robot will be fabricated and motion control methods are to be studied.

ACKNOWLEDGEMENT

The authors would like to thank Tokyo Sea Life Park for providing the wing sample, and Tatsushi Yamada who contributed to the measurement of the wing.

REFERENCES

[1] Q. Zhong, J. Zhu, F. E. Fish, S. J. Kerr, A. Downs, H. Bart-Smith, and D. Quinn, "Tunable stiffness enables fast and efficient swimming in fish-like robots," *Science Robotics*, vol. 6, no. 57, p. eabe4088, 2021.

[2] D. Chen, Z. Wu, Y. Meng, M. Tan, and J. Yu, "Development of a high-speed swimming robot with the capability of fish-like leaping," *IEEE/ASME Transactions on Mechatronics*, vol. 27, no. 5, pp. 3579–3589, 2022.

[3] J. Lou, T. Gu, T. Chen, Y. Yang, C. Xu, Y. Wei, and Y. Cui, "Effects of actuator-substrate ratio on hydrodynamic and propulsion performances of underwater oscillating flexible structure actuated by macro fiber composites," *Mechanical Systems and Signal Processing*, vol. 170, p. 108824, 2022.

[4] Y. Liu, H. Li, S. Deng, S. Wang, S. Liu, and Z. Wang, "Biomimetic robotic sea lion foreflippers: Design, modeling, and experimentation," *IEEE/ASME Transactions on Mechatronics*, vol. 27, no. 6, pp. 5679–5689, 2022.

[5] J.-Y. Cheng, L.-X. Zhuang, and B.-G. Tong, "Analysis of swimming three-dimensional waving plates," *Journal of Fluid Mechanics*, vol. 232, pp. 341–355, 1991.

[6] R. J. Raikow, L. Bicanovsky, and A. H. Bledsoe, "Forelimb joint mobility and the evolution of wing-propelled diving in birds," *The Auk*, vol. 105, no. 3, pp. 446–451, 1988.

[7] R. Bannasch, "Hydrodynamics of penguins-an experimental approach," *The Penguins; Ecology and Management*, pp. 141–176, 1995.

[8] M. C. DeBlois and R. Motani, "Flipper bone distribution reveals flexible trailing edge in underwater flying marine tetrapods," *Journal of Morphology*, vol. 280, no. 6, pp. 908–924, 2019.

[9] R. Bannasch, "Functional anatomy of the flight apparatus in penguins," in *mechanics and physiology of animal swimming*, 1994, pp. 163–192.

[10] K. Sato, Y. Naito, A. Kato, Y. Niizuma, Y. Watanuki, J.-B. Charrassin, C.-A. Bost, Y. Handrich, and Y. Le Maho, "Buoyancy and maximal diving depth in penguins: do they control inhaling air volume?" *Journal of Experimental Biology*, vol. 205, no. 9, pp. 1189–1197, 2002.

[11] K. Sato, Y. Watanuki, A. Takahashi, P. J. Miller, H. Tanaka, R. Kawabe, P. J. Ponganis, Y. Handrich, T. Akamatsu, Y. Watanabe *et al.*, "Stroke frequency, but not swimming speed, is related to body size in free-ranging seabirds, pinnipeds and cetaceans," *Proceedings of the Royal Society B: Biological Sciences*, vol. 274, no. 1609, pp. 471–477, 2007.

[12] Y. Watanuki, S. Wanless, M. Harris, J. R. Lovvorn, M. Miyazaki, H. Tanaka, and K. Sato, "Swim speeds and stroke patterns in wing-propelled divers: a comparison among alcids and a penguin," *Journal of Experimental biology*, vol. 209, no. 7, pp. 1217–1230, 2006.

[13] B. D. Clark and W. Bemis, "Kinematics of swimming of penguins at the detroit zoo," *Journal of Zoology*, vol. 188, no. 3, pp. 411–428, 1979.

[14] C. A. Hui, "Penguin swimming. i. hydrodynamics," *Physiological zoology*, vol. 61, no. 4, pp. 333–343, 1988.

[15] C. A. Hui, "Penguin swimming. ii. energetics and behavior," *Physiological Zoology*, vol. 61, no. 4, pp. 344–350, 1988.

[16] N. Harada, T. Oura, M. Maeda, Y. Shen, D. M. Kikuchi, and H. Tanaka, "Kinematics and hydrodynamics analyses of swimming penguins: wing bending improves propulsion performance," *Journal of Experimental Biology*, vol. 224, no. 21, p. jeb242140, 2021.

[17] Y. Shen and H. Tanaka, "Experimental analysis of the sweepback angle effect on the thrust generation of a robotic penguin wing," *Bioinspiration & Biomimetics*, 2023.

[18] Y. Shen, N. Harada, S. Katagiri, and H. Tanaka, "Biomimetic realization of a robotic penguin wing: Design and thrust characteristics," *IEEE/ASME Transactions on Mechatronics*, vol. 26, no. 5, pp. 2350–2361, 2020.

[19] W. Wang, X. Dai, L. Li, B. H. Gheneti, Y. Ding, J. Yu, and G. Xie, "Three-dimensional modeling of a fin-actuated robotic fish with multimodal swimming," *IEEE/ASME Transactions on Mechatronics*, vol. 23, no. 4, pp. 1641–1652, 2018.

[20] F. E. Fish, "Advantages of natural propulsive systems," *Marine Technology Society Journal*, vol. 47, no. 5, 2013.

[21] P. R. Bandyopadhyay, "Trends in biorobotic autonomous undersea vehicles," *IEEE Journal of Oceanic Engineering*, vol. 30, no. 1, pp. 109–139, 2005.

[22] V. Kopman and M. Porfiri, "Design, modeling, and characterization of a miniature robotic fish for research and education in biomimetics and bioinspiration," *IEEE/ASME Transactions on mechatronics*, vol. 18, no. 2, pp. 471–483, 2012.

[23] Y.-J. Park, T. M. Huh, D. Park, and K.-J. Cho, "Design of a variable-stiffness flapping mechanism for maximizing the thrust of a bio-inspired underwater robot," *Bioinspiration & biomimetics*, vol. 9, no. 3, p. 036002, 2014.

[24] F. Zhang, O. Ennasr, E. Litchman, and X. Tan, "Autonomous sampling of water columns using gliding robotic fish: Algorithms and harmful-algae-sampling experiments," *IEEE Systems Journal*, vol. 10, no. 3, pp. 1271–1281, 2015.

[25] R. K. Katzschmann, J. DelPreto, R. MacCurdy, and D. Rus, "Exploration of underwater life with an acoustically controlled soft robotic fish," *Science Robotics*, vol. 3, no. 16, p. eaar3449, 2018.

[26] P. Kodati, J. Hinkle, A. Winn, and X. Deng, "Microautonomous robotic ostraciiform (marco): Hydrodynamics, design, and fabrication," *IEEE Transactions on Robotics*, vol. 24, no. 1, pp. 105–117, 2008.

[27] S. Zhang, Y. Qian, P. Liao, F. Qin, and J. Yang, "Design and control of an agile robotic fish with integrative biomimetic mechanisms," *IEEE/ASME Transactions on Mechatronics*, vol. 21, no. 4, pp. 1846–1857, 2016.

[28] W. Stoll, "Aquapenguin," Technical report, FESTO, Tech. Rep., 2009.

[29] N. Harada and H. Tanaka, "Kinematic and hydrodynamic analyses of turning manoeuvres in penguins: body banking and wing upstroke generate centripetal force," *Journal of Experimental Biology*, vol. 225, no. 24, p. jeb244124, 2022.